Polymer 55 (2014) 6058–6068

Contents lists available at ScienceDirect

Polymer

journal homepage: www.elsevier.com/locate/polymer

Synthesis of hyperbranched polythiophenes containing tetrachloroperylene bisimide as bridging moiety for polymer solar cells

Sheng-Hsiung Yang [a, *], Tz-Shiuan Lin [a], Yu-Zhang Huang [b], Husan-De Li [b], Yu-Chiang Chao [b, **]

[a] Institute of Lighting and Energy Photonics, National Chiao Tung University, No. 301, Gaofa 3rd Road, Guiren Dist., Tainan 71150, Taiwan ROC
[b] Department of Physics, Chung-Yuan Christian University, No. 200, Chung-Pei Road, Chung-Li 32023, Taiwan ROC

ARTICLE INFO

Article history:
Received 7 April 2014
Received in revised form
6 August 2014
Accepted 17 September 2014
Available online 26 September 2014

Keywords:
Hyperbranched
Polythiophene
Tetrachloroperylene bisimide

ABSTRACT

The goal of this research is to synthesize the hyperbranched polythiophene derivatives (**P1** and **P4**) containing tetrachloroperylene bisimide as bridging moiety for investigation of thermal, electrochemical, and opto-electrical properties of these derivatives. The polymers (**P2** and **P3**) containing soft alkyl spacer as bridging moiety and linear poly(3-hexylthiophene) (P3HT) were also synthesized for comparison in this study. Polymers with high regioregularity were synthesized via the Universal Grignard metathesis polymerization. The GPC results showed that molecular weights of hyperbranched polythiophenes are higher than that of P3HT. The TGA experiments revealed a first-stage weight loss at about 300 °C for all polymers; besides, polymers containing rigid tetrachloroperylene bisimide groups possess less weight loss than P3HT after heating, indicative of enhanced thermal stabilities. The UV–vis absorption maxima of hyperbranched polymers are similar to that of P3HT in film state, while their absorption shoulder bands are stronger than that of P3HT, indicating stronger interchain interaction and shorter distance between backbones by the introduction of bridge architecture. Moreover, an attenuation of fluorescent intensity was found for those hyperbranched polymers, implying reduced recombination of excitons to emit light and more opportunity for carriers to migrate to both electrodes. Electrochemical analysis showed that introducing hyperbranched structure resulted in decreasing both LUMO and HOMO levels of polymers. All polymers were used for fabrication of polymer solar cells with the configuration of ITO/PEDOT/polymer:$PC_{60}BM$ (1:2 w/w)/LiF/Al to evaluate their performance. The power conversion efficiency (PCE) of the P3HT:$PC_{60}BM$-based device is 0.54%, while devices based on hyperbranched polymers showed *PCE* values in the range of 0.45–0.84%. The morphological study of polymer:$PC_{60}BM$ blend films was performed by AFM for interpretation of efficiency trend of devices.

1. Introduction

Polythiophene (PT) and its derivatives, especially poly(3-hexylthiophene) (P3HT), have been used for fabrication of organic optoelectronics because of good thermal and chemical stability, and excellent opto-electrical properties. McCullough et al. firstly proposed P3HT with >95% regioregularity by metathesis polymerization [1,2]. The highly ordered head-to-tail structure makes close packing between P3HT main chains and increased absorption in the red-light region. A thin film made of a PT derivative with thioalkyl side groups was also found to enhance its electrical conductivity by exposure to laser radiation [3]. Polymer solar cells based on P3HT achieved power conversion efficiency (PCE) of 4.3% with suitable thermal annealing technique [4]. The polymer microstructure and polymer:fullerene blend morphology were recognized and discussed for production of high photovoltaic performance [5]. Main-chain type PTs have widely been developed in the literature [6], while side-chain PTs are less reported. Wei et al. reported an intramolecular donor–acceptor regioregular side-chain PT derivative (PHPIP) by incorporating electron-deficient phenanthrenyl-imidazole group as side pendant [7,8]. They proposed that charge dissociation may occur on the interface between PT main chain and side pendants, allowing electrons to transport from phenanthrenyl-

* Corresponding author. Tel.: +886 6 3032121; fax: +886 6 3032535.
** Corresponding author. Tel.: +886 3 2653208; fax: +886 3 2653299.
E-mail addresses: yangsh@mail.nctu.edu.tw (S.-H. Yang), ycchao@cycu.edu.tw (Y.-C. Chao).

http://dx.doi.org/10.1016/j.polymer.2014.09.046
0032-3861/

imidazole group to [6,6]phenyl-C_{61}-butyric acid methyl ester ($PC_{60}BM$), while holes migrate along PT main chains. The solar device based on PHPIP:$PC_{60}BM$ led to a short-circuit current density (J_{SC}) of 11.3 mA/cm^2 and a PCE value of 4.1%. Li et al. reported a side-chain PT copolymer (PT-VTVTC12) containing bi(thienylene-vinylene) side chains to increase light absorption in the ultraviolet region [9]. The solar device based on PT-VTVTC12:$PC_{60}BM$ reached a PCE value of 3.18%. Lanzi et al. reported a new PT-based double-cable polymer with pendent C_{60}-fullerene group [10]. The solar device based on this C_{60}-fullerene-containing copolymer showed a PCE value of 1.55%. An even higher PCE value of 2.24% was obtained by using the fullerene-functionalized monomer in blend with P3HT instead of the usually employed $PC_{60}BM$. Emrick et al. reported a P3HT derivative containing perylene bisimide (PBI) as side pendent [11]. The photoluminescence intensity of the side-chain type P3HT was decreased compared to linear P3HT, indicating increased aggregation of polymer chains. However, the PCE value of solar device was low (0.49%).

Apart from main-chain and side-chain type P3HTs, π-bridged P3HTs have also been studied to investigate the effect of bridging moieties on the performance of final polymers. Li et al. designed a terthiophene-bridged P3HT derivative (PT-VTThV) by incorporating divinyl-terthiophene moiety between P3HT main chains to elongate conjugation length [12]. They proposed that charge carriers could migrate in two ways: along one single chain and through bridging moiety to another polymer chain. The hole mobility of the polymer was increased by experimental measurement. The performance of solar device based on PT-VTThV:$PC_{60}BM$ was less promoted (PCE = 1.72%). Tu et al. reported another bridged P3HT (B-P3HT) by using 3,3′-dithiophene as bridging moiety [13]. The distance between two bridged P3HT chains was reduced compared to previous example PT-VTThV; however, the hole mobility of polymer was decreased. The PCE values of solar devices based on B-P3HT:$PC_{60}BM$ were 0.13–2%. Mangold et al. reported two hyperbranched PTs using 2,3-dithienylthiophene or 2,3,5-trithienylthiophene as bridging cores [14]. The optimized solar cell based on the hyperbranched PT material in combination with $PC_{60}BM$ showed an open-circuit voltage (V_{OC}) 30% higher (up to 714 mV) than normally found with P3HT. The PCE values of solar devices were measured to be 0.58–0.61%.

In this study, we propose a new approach to synthesize the hyperbranched PT derivatives by introducing perylene bisimide (PBI) or soft alkyl spacer as bridging moieties. PBI is a well-known electron-withdrawing material, which may contribute to charge dissociation in a donor–acceptor polymer. Four chlorine atoms are designed to introduce on bay positions of perylene core to improve solubility of intermediates and final polymers [15]. To obtain hyperbranched polymers, four different two-headed monomers containing tetrachloroperylene bisimide or alkyl spacer were synthesized and added during polymerization of P3HT. The synthesized polymers are expected to form hyperbranched structure, accompanying with increased molecular weights and improved thermal properties. Linear P3HT was also prepared according to the same polymerization condition for comparison. The electrical and spectroscopic properties of theses polymers were systematically investigated. In addition, polymer solar devices were also fabricated to evaluate performance of the polymers.

2. Experimental

2.1. Characterization methods

The synthesized materials were characterized by the following techniques. ^{1}H and ^{13}C NMR spectra were recorded on a Bruker Avance 600 MHz NMR spectrometer. Mass spectra were recorded on a Micromass TRIO-2000 GC–MS instrument, using electron impact (EI) or fast atom bombardment (FAB) as ionization source. Gel permeation chromatography (GPC) data assembled from Viscotek with a VE3850 RI detector and three columns in series were used to measure molecular weights relative to polystyrene standards at 32 °C. Differential scanning calorimetry (DSC) was performed on a Seiko DSC 6200 unit at a heating rate of 10 °C/min. Thermogravimetric analysis (TGA) was undertaken on a Seiko TG/DTA 7200 instrument at a heating rate of 10 °C/min. UV–vis absorption and photoluminescence (PL) spectra were obtained with a Princeton Instruments Acton 2150 spectrophotometer. Cyclic voltammetric measurements of materials were made in acetonitrile with 0.1 M tetrabutylammonium tetrafluoroborate ($TBABF_4$) as the supporting electrolyte at a scan rate of 50 mV/s. Indium–tin oxide (ITO) electrodes were used as both the working and counter electrodes, and silver/silver ions (Ag in 0.1 M $AgNO_3$ solution, from Bioanalytical Systems, Inc.) was used as the reference electrode. Ferrocene was used as an internal standard, and the potential values were obtained and converted to vs SCE (saturated calomel electrode). The corresponding highest-occupied molecular orbital (HOMO) was estimated from the onset of oxidation potential. Atomic force microscopy (AFM) experiments were performed on a Bruker Innova AFM for detecting surfaces morphologies of polymer blend films.

2.2. Synthesis of monomers

The synthetic routes to intermediates and two-headed monomers **M1**–**M4** are shown in Schemes 1 and 2. The monomer 2,5-Dibromo-3-hexylthiophene (**M5**) was prepared according to the previous literature [16]. Detailed synthetic procedures are described as follows.

2.2.1. 1,6,7,12-tetrachloro-3,4,9,10-perylenetetracarboxylic dianhydride (1)

A mixture of 3,4,9,10-perylenetetracarboxylic dianhydride (3.30 g, 8.41 mmol), chlorosulfonic acid (20 mL, 300 mmol) and iodine (0.56 g, 2.20 mmol) was stirred at 65 °C for 30 h. After cooling to room temperature, the solution was added dropwise to an ice-water mixture. The precipitate was collected by filtration to give a red solid (4.14 g, 92%). ^{1}H NMR (*d*-DMSO, ppm): 8.75 (s, 4H, aromatic protons). ^{13}C NMR (*d*-DMSO, ppm): 119.75, 125.29, 129.5, 134.88, 136.22, 158.16, 168.53. Mass (EI): *m*/*z* 532.

2.2.2. 1-(6′-bromohexyloxy)-4-methoxybenzene (2)

A solution of 4-methoxyphenol (10.0 g, 80.58 mmol), 1,6-dibromohexane (60.0 g, 245.90 mmol), and potassium hydroxide (6.0 g, 106.95 mmol) in 100 mL of dimethyl sulfoxide (DMSO) was stirred at room temperature for 6 h. The solution was extracted with dichloromethane (DCM) and water, and the organic phase was dried with anhydrous $MgSO_4$. The crude product was concentrated in vacuo and purified by gel chromatography (silica gel, DCM/hexane = 2/1 in volume ratio as the eluant) to give a white solid (15.0 g, 65%). ^{1}H NMR ($CDCl_3$, ppm): 1.46–1.51 (m, 4H, $-OCH_2CH_2(CH_2)_2-CH_2CH_2Br$), 1.76–1.81 (m, 2H, $-CH_2CH_2Br$), 1.87–1.91 (m, 2H, $-OCH_2CH_2-$), 3.40–3.44 (m, 2H, $-CH_2Br$), 3.77 (s, 3H, $-OCH_3$), 3.90–3.93 (t, J = 6.0 Hz, 2H, $-OCH_2-$), 6.83 (s, 4H, aromatic protons). ^{13}C NMR ($CDCl_3$, ppm): 25.32, 27.94, 29.21, 32.70, 33.78, 55.75, 68.41, 114.65, 115.46, 153.22, 153.75. MASS (EI): *m*/*z* 287.

2.2.3. 1-(6′-bromohexyloxy)-2,5-dibromo-4-methoxybenzene (3)

A solution of liquid bromine (8.0 g, 50.0 mmol) in 30 mL of $CHCl_3$ was added dropwise to a mixture of **(2)** (5.0 g, 17.41 mmol), a catalytic amount of iron powder, and 240 mL of $CHCl_3$ at 0 °C. The

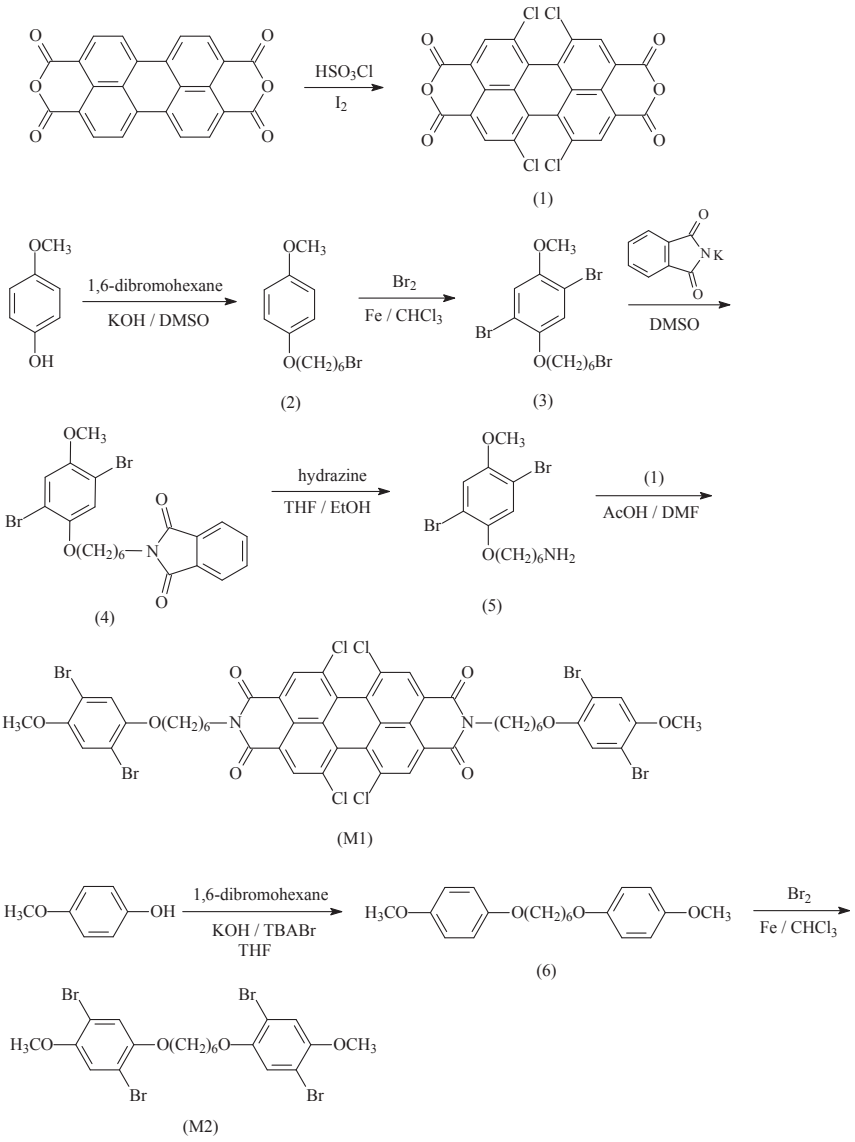

Scheme 1. Synthesis of monomers M1 and M2.

solution was then stirred at room temperature for 12 h. After extracting with water twice, the organic phase was collected and dried with anhydrous $MgSO_4$. The crude product was concentrated in vacuo and purified by gel chromatography (silica gel, ethyl acetate/hexane = 1/14 in volume ratio as the eluant) to give a white solid (5.0 g, 65%). ^{1}H NMR ($CDCl_3$, ppm): 1.52–1.54 (t, J = 3.5 Hz, 4H, $-OCH_2-$ $CH_2(CH_2)_2CH_2CH_2Br$), 1.79–1.85 (m, 2H, $-CH_2CH_2Br$), 1.88–1.93 (m, 2H, $-OCH_2CH_2-$), 3.41–3.44 (t, J = 6.7 Hz, 2H, $-CH_2Br$), 3.84 (s, 3H, $-OCH_3$), 3.94–3.97 (t, J = 6.3 Hz, 2H, $-OCH_2-$), 7.09 (s, 2H, aromatic protons). ^{13}C NMR ($CDCl_3$, ppm): 25.19, 27.81, 28.92, 32.64, 33.74, 56.99, 70.06, 110.41, 111.27, 117.01, 118.65, 150.04, 150.55. MASS (EI): m/z 445.

2.2.4. N-[6-(2,5-dibromo-4-methoxyphenyl)hexyl]phthalimide (4)

A solution of **(3)** (2.0 g, 4.49 mmol), and potassium phthalimide (1.10 g, 5.94 mmol) in 30 mL of DMSO was stirred at 70 °C for 16 h. The solution was extracted with ethyl acetate and water, and the organic phase was collected and dried with anhydrous $MgSO_4$. The crude product was concentrated in vacuo and purified by gel chromatography (silica gel, DCM as the eluant) to give a white solid (1.50 g, 65%). ^{1}H NMR ($CDCl_3$, ppm): 1.40–1.46 (m, 2H, $-OCH_2CH_2-CH_2CH_2CH_2CH_2N-$), 1.51–1.57 (m, 2H, $-OCH_2CH_2CH_2CH_2CH_2CH_2N-$), 1.69–1.75 (m, 2H, $-CH_2CH_2N-$), 1.77–1.83 (m, 2H, $-OCH_2CH_2-$), 3.68–3.71 (t, J = 7.2 Hz, 2H, $-CH_2N-$), 3.83 (s, 3H, $-OCH_3$), 3.92–3.95 (t, J = 6.4 Hz, 2H, $-OCH_2-$), 7.07 (s, 2H, aromatic protons), 7.69–7.71 (dd, J_1 = 5.3 Hz, J_2 = 3.0 Hz, 2H, aromatic protons), 7.82–7.84 (dd, J_1 = 5.3 Hz, J_2 = 3.0 Hz, 2H, aromatic protons). ^{13}C NMR ($CDCl_3$, ppm): 25.58, 26.51, 28.50, 28.94, 37.88, 56.98, 70.10, 110.36, 111.24, 117.01, 118.57, 123.15, 132.14, 133.83, 150.07, 150.47, 168.44. MASS (EI): m/z 511.

2.2.5. N-(6-aminohexyl)-2,5-dibromo-4-methoxybenzene (5)

A solution of **(4)** (2.0 g, 3.91 mmol) and hydrazine (2.40 g, 31.30 mmol) in a solvent mixture of ethanol (20 mL) and tetrahydrofuran (THF, 20 mL) was refluxed at 70 °C for 4 h. The solution was then extracted with ethyl acetate and water, and the organic phase was dried with anhydrous $MgSO_4$. The crude product was concentrated in vacuo and purified by gel chromatography (silica gel, methanol as the eluant) to give a yellowish viscous liquid (1.10 g, 74%). ^{1}H NMR ($CDCl_3$, ppm): 1.39–1.44 (m, 2H,

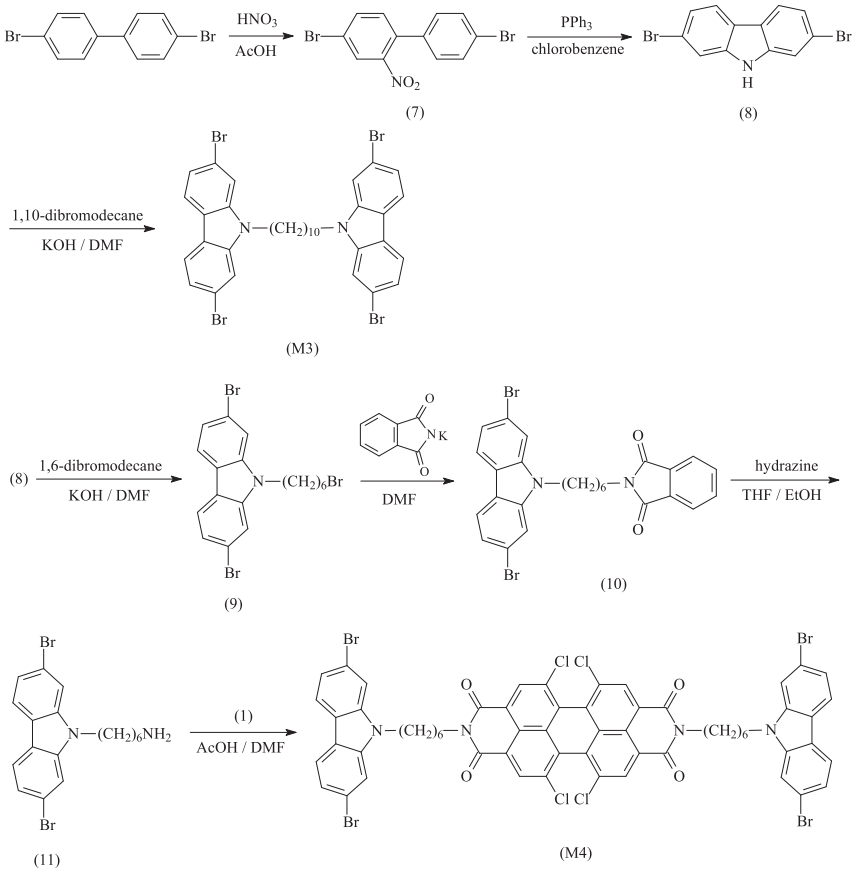

Scheme 2. Synthesis of monomers M3 and M4.

$-OCH_2CH_2CH_2\underline{C}H_2CH_2CH_2NH_2$), 1.48–1.55 (m, 4H, $-OCH_2CH_2\underline{C}H_2CH_2-$ $C\underline{H}_2CH_2NH_2$), 1.76 (s, 2H, $-NH_2$), 1.79–1.84 (m, 2H, $-OCH_2C\underline{H}_2-$), 2.71–2.74 (t, J = 7.0 Hz, 2H, $-C\underline{H}_2NH_2$), 3.84 (s, 3H, $-OC\underline{H}_3$), 3.94–3.97 (t, J = 6.4 Hz, 2H, $-OC\underline{H}_2-$), 7.09 (s, 2H, aromatic protons). ^{13}C NMR ($CDCl_3$, ppm): 25.82, 26.53, 29.08, 33.34, 41.99, 57.00, 70.23, 110.43, 111.28, 117.06, 118.68, 150.13, 150.54. MASS (EI): m/z 381.

2.2.6. *N,N′-bis[6-(2,5-dibromo-4-methoxyphenyl)hexyl]-1,6,7,12-tetrachloro-3,4,9,10-perylenetetracarboxylic bisimide **(M1)***

A solution of **(1)** (0.39 g, 7.33 mmol), **(5)** (1.1 g, 29.32 mmol), and glacial acetic acid (11 mL) in 55 mL of *N,N*-dimethylformamide (DMF) was stirred at 80 °C for 18 h. The reaction mixture was cooled to room temperature and poured into an ice-water mixture. The precipitate was collected, washed with excess of water, and separated by gel chromatography (silica gel, DCM as the eluant). The concentrated product was further re-precipitated twice in DCM (20 mL)/hexane (50 mL) solvent mixture to yield a red solid (0.59 g, 65%). ^{1}H NMR ($CDCl_3$, ppm): 1.50–1.63 (m, 8H, $-OCH_2CH_2-C\underline{H}_2C\underline{H}_2CH_2CH_2-$perylene), 1.77–1.87 (m, 8H, $-OCH_2C\underline{H}_2CH_2CH_2-C\underline{H}_2CH_2-$perylene), 3.83 (s, 6H, $-OC\underline{H}_3$), 3.95–3.98 (t, J = 6.3 Hz, 4H, $-OC\underline{H}_2-$), 4.22–4.25 (t, J = 7.4 Hz, 4H, $-C\underline{H}_2-$perylene), 7.07 (s, 2H, aromatic protons), 7.09 (s, 2H, aromatic protons), 8.68 (s, 4H, aromatic protons). ^{13}C NMR ($CDCl_3$, ppm): 25.71, 26.71, 27.98, 28.96, 29.68, 40.78, 56.98, 70.13, 110.39, 111.24, 117.00, 118.58, 123.21, 123.26, 128.59, 131.94, 132.94, 135.36, 150.07, 150.48, 162.24. MASS (FAB): m/z 1258.

2.2.7. *1-[6-(4-methoxyphenoxy)hexyloxy]-4-methoxybenzene **(6)***

A solution of 4-methoxyphenol (9.0 g, 72.5 mmol), 1,6-dibromohexane (8.1 g, 33.2 mmol), potassium hydroxide (5.4 g, 96.3 mmol), and a catalytic amount of tetrabutylammonium bromide in 150 mL of THF was refluxed at 70 °C for 12 h. After cooling to room temperature, the solution was poured into water. The precipitate was collected by filtration and washed with ethyl acetate and hexane to give a white solid (6.0 g, 84%). ^{1}H NMR ($CDCl_3$, ppm): 1.59–1.58 (m, 4H, $-OCH_2CH_2-$ $C\underline{H}_2C\underline{H}_2CH_2CH_2O-$), 1.88–1.84 (m, 4H, $-OCH_2C\underline{H}_2CH_2CH_2C\underline{H}_2CH_2O-$), 3.77 (s, 6H, $-OC\underline{H}_3$), 3.93–3.91 (t, J = 6.0 Hz, 4H, $-OC\underline{H}_2(CH_2)_4C\underline{H}_2O-$), 6.83 (s, 8H, aromatic protons). ^{13}C NMR ($CDCl_3$, ppm): 25.88, 29.33, 55.74, 68.51, 114.63, 115.45, 153.27, 153.71. Mass (EI): m/z 330.

2.2.8. *1-[6-(2,5-dibromo-4-methoxyphenyl)hexyloxy]-2,5-dibromo-4-methoxybenzene **(M2)***

A solution of liquid bromine (9.0 g, 56.25 mmol) in 10 mL of $CHCl_3$ was added dropwise to a mixture of **(6)** (4.0 g, 12.11 mmol) and a catalytic amount of iron powder in 240 mL of $CHCl_3$ at 0 °C. The solution was stirred at room temperature for 12 h. The solution was then extracted with water twice, and the organic phase was dried with anhydrous $MgSO_4$. The crude product was concentrated in vacuo and purified by gel chromatography (silica gel, DCM/hexane = 3/2 in volume ratio as the eluant) to give a white solid (0.8 g, 10%). ^{1}H NMR ($CDCl_3$, ppm): 1.57–1.60 (m, 4H, $-OCH_2CH_2-C\underline{H}_2C\underline{H}_2CH_2CH_2O-$), 1.82–1.86 (m, 4H, $-OCH_2C\underline{H}_2CH_2-CH_2C\underline{H}_2CH_2O-$), 3.84 (s, 6H, $-OC\underline{H}_3$), 3.96–3.99 (t, 4H, J = 6.0 Hz, $-OC\underline{H}_2(CH_2)_4C\underline{H}_2O-$), 7.08 (s, 2H, aromatic protons), 7.09 (s, 2H, aromatic protons). ^{13}C NMR ($CDCl_3$, ppm): 25.43, 28.94, 55.96, 69.97, 110.37, 111.23, 116.96, 118.56, 150.06, 150.47. Mass (EI): m/z 646.

2.2.9. *4,4′-dibromo-2-nitrobiphenyl **(7)***

A solution of 4,4′-dibromobiphenyl (5.0 g, 16.03 mmol) in 75 mL of glacial acetic acid was heated to 100 °C, and then 60 mL of nitric

acid was added dropwise. The solution was stirred at 100 °C for 12 h. After cooling to room temperature, the reaction mixture was poured into an ice-water mixture. The precipitate was collected by filtration, washed with excess of water, and purified by gel chromatography (silica gel, ethyl acetate/hexane = 1/10 in volume ratio as the eluant) to give a yellow solid (5.03 g, 88%). ^{1}H NMR ($CDCl_3$, ppm): 7.14 (d, J = 8.0 Hz, 1H, aromatic proton), 7.27 (d, J = 8.0 Hz, 1H, aromatic proton), 7.55 (d, J = 8.0 Hz, 1H, aromatic proton), 7.74 (dd, J_1 = 8.0 Hz, J_2 = 2.0 Hz, 1H, aromatic proton), 8.02 (d, J = 2.0 Hz, 1H, aromatic proton). ^{13}C NMR ($CDCl_3$, ppm): 121.78, 123.01, 127.21, 128.43, 128.46, 129.37, 131.97, 132.98, 134.08, 135.25, 135.52, 149.20. MASS (EI): m/z 357.

2.2.10. 2,7-dibromocarbazole **(8)**

A solution of **(7)** (4.0 g, 11.21 mmol) and triphenylphosphine (7.20 g, 27.45 mmol) in 45 mL of chlorobenzene was stirred at 120 °C for 16 h. The solution was extracted with ethyl acetate and water, and the organic phase was dried with anhydrous $MgSO_4$. The crude product was concentrated in vacuo and purified by gel chromatography (silica gel, DCM/hexane = 1/2 in volume ratio as the eluant) to give a white solid (1.86 g, 51%). ^{1}H NMR ($CDCl_3$, ppm): 7.35–7.36 (d, J = 8.0 Hz, 2H, aromatic protons), 7.58 (s, 2H, aromatic protons), 7.86–7.88 (d, J = 8.0 Hz, 2H, aromatic protons), 8.10 (s, 1H, $-$NH). ^{13}C NMR ($CDCl_3$, ppm): 113.83, 119.73, 121.45, 121.79, 132.29, 140.29. MASS (EI): m/z 325.

2.2.11. N-[10-(2,7-dibromocarbazolyl)decyl]-2,7-dibromocarbazole **(M3)**

A mixture of **(8)** (1.0 g, 72.5 mmol), 1,10-dibromodecane (0.46 g, 1.53 mmol), potassium hydroxide (0.8 g, 14.29 mmol), and a catalytic amount of tetrabutylammonium bromide in 20 mL of DMF was stirred at room temperature for 24 h. The reaction mixture was then poured into water, and the precipitate was collected by filtration and washed with ethyl acetate and hexane to give a white solid (0.62 g, 52%). ^{1}H NMR ($CDCl_3$, ppm): 1.22–1.35 (m, 12H, $-NCH_2CH_2-(CH_2)_6CH_2CH_2N-$), 1.78–1.84 (m, 4H, $-NCH_2CH_2-$), 4.15–4.18 (t, J = 7.0 Hz, 4H, $-NCH_2-$), 7.31–7.33 (d, J = 8.0 Hz, 4H, aromatic protons), 7.48 (s, 4H, aromatic protons), 7.86–7.88 (d, J = 8.0 Hz, 4H, aromatic protons). ^{13}C NMR ($CDCl_3$, ppm): 27.04, 28.68, 29.18, 29.23, 43.16, 112.00, 119.68, 121.27, 121.47, 122.52, 141.35. MASS (EI): m/z 788.

2.2.12. N-(6-bromohexyl)-2,7-dibromocarbazole **(9)**

A mixture of **(8)** (2.0 g, 6.16 mmol), 1,6-dibromohexane (3.0 g, 12.3 mmol), and potassium hydroxide (0.4 g, 7.13 mmol) in 40 mL of DMF was stirred at room temperature for 24 h. The solution was then extracted with ethyl acetate and water, and the organic phase was dried with anhydrous $MgSO_4$. The crude product was concentrated in vacuo and purified by gel chromatography (silica gel, DCM/hexane = 1/5 in volume ratio as the eluant) to give a white solid (0.93 g, 30%). ^{1}H NMR ($CDCl_3$, ppm): 1.36–1.41 (m, 2H, $-NCH_2CH_2CH_2-CH_2CH_2CH_2Br$), 1.47–1.52 (m, 2H, $-NCH_2CH_2CH_2CH_2-$ CH_2CH_2Br), 1.81–1.88 (m, 4H, $-NCH_2CH_2CH_2CH_2CH_2CH_2Br$), 3.36–3.39 (t, J = 7.0 Hz, 2H, $-CH_2Br$), 4.16–4.19 (t, J = 7.0 Hz, 2H, $-NCH_2-$), 7.33–7.35 (d, J = 8.0 Hz, 2H, aromatic protons), 7.51 (s, 2H, aromatic protons), 7.86–7.88 (t, 2H, J = 8.0 Hz, aromatic protons). ^{13}C NMR ($CDCl_3$, ppm): 26.34, 27.84, 28.61, 32.50, 33.56, 43.12, 111.92, 119.72, 121.28, 121.49, 122.60, 141.29. MASS (EI): m/z 486.

2.2.13. N-[6-(2,7-dibromocarbazolyl)hexyl]phthalimide **(10)**

A mixture of **(9)** (0.1 g, 0.21 mmol) and potassium phthalimide (0.042 g, 0.23 mmol) in 5 mL of DMF was stirred at 70 °C for 16 h. The mixture was then extracted with ethyl acetate and water, and the organic phase was dried with anhydrous $MgSO_4$. The crude product was concentrated in vacuo and purified by gel chromatography (silica gel, DCM as the eluant) to give a white solid (0.08 g, 71%). ^{1}H NMR ($CDCl_3$, ppm): 1.37–1.45 (m, 4H, carbazole$-CH_2CH_2-CH_2CH_2CH_2CH_2N-$), 1.65–1.70 (m, 2H, carbazole$-CH_2CH_2-$), 1.82–1.87 (m, 2H, $-CH_2CH_2N-$), 3.66–3.69 (t, J = 7.0 Hz, 2H, carbazole$-CH_2-$), 4.18–4.21 (t, J = 7.0 Hz, 2H, $-CH_2N-$), 7.32–7.34 (dd, J_1 = 8.0 Hz, J_2 = 1.0 Hz, 2H, aromatic protons), 7.51 (d, J = 1.0 Hz, 2H, aromatic protons), 7.69–7.71 (dd, J_1 = 6.0 Hz, J_2 = 3.0 Hz, 2H, aromatic protons), 7.82–7.84 (dd, J_1 = 6.0 Hz, J_2 = 3.0 Hz, 2H, aromatic protons), 7.87–7.89 (d, J = 8.0 Hz, 2H, aromatic protons). ^{13}C NMR ($CDCl_3$, ppm): 26.75, 28.43, 28.70, 29.69, 37.75, 43.26, 111.97, 119.72, 121.30, 121.48, 122.58, 123.19, 132.13, 133.87, 141.32, 168.41. MASS (EI): m/z 553.

2.2.14. N-(6-aminohexyl)-2,7-dibromocarbazole **(11)**

A solution of **(10)** (0.1 g, 0.18 mmol) and hydrazine (0.01 g, 0.56 mmol) in a solvent mixture of ethanol (5 mL) and THF (55 mL) was refluxed at 70 °C for 4 h. The solution was then extracted with ethyl acetate and water, and the organic phase was dried with anhydrous $MgSO_4$. The crude product was concentrated in vacuo and purified by gel chromatography (silica gel, methanol as the eluant) to give a yellowish viscous liquid (0.02 g, 27%). ^{1}H NMR ($CDCl_3$, ppm): 1.37 (m, 6H, $-NCH_2CH_2CH_2CH_2CH_2CH_2NH_2$), 1.84 (m, 2H, $-NCH_2CH_2-$), 1.95 (m, 2H, $-CH_2NH_2$), 2.71 (s, 2H, $-NH_2$), 4.16–4.19 (t, J = 7.0 Hz, 2H, $-NCH_2-$), 7.32–7.34 (d, J = 8.0 Hz, 2H, aromatic protons), 7.51 (s, 2H, aromatic protons), 7.87–7.88 (d, 2H, J = 8.0 Hz, aromatic protons). ^{13}C NMR ($CDCl_3$, ppm): 26.55, 26.96, 28.73, 29.67, 43.22, 111.95, 119.68, 121.26, 121.48, 122.54, 141.32. MASS (EI): m/z 424.

2.2.15. N,N′-bis[6-(2,7-dibromocarbazolyl)hexyl]-1,6,7,12-tetrachloro-3,4,9,10-perylene tetracarboxylic bisimide **(M4)**

A mixture of **(1)** (0.1 g, 0.19 mmol), **(11)** (0.32 g, 0.75 mmol), and glacial acetic acid (1 mL) in 10 mL of DMF was stirred at 80 °C for 18 h. The reaction mixture was cooled to room temperature and poured into an ice-water mixture. The precipitate was collected, washed with excess of water, and separated by gel chromatography (silica gel, DCM/hexane = 1/2 in volume ratio as the eluant). The concentrated product was further re-precipitated twice in DCM (20 mL)/hexane (50 mL) solvent mixture to yield a mauve solid (0.015 g, 6%). ^{1}H NMR ($CDCl_3$, ppm): 1.48 (m, 8H, $-NCH_2CH_2-(CH_2)_2CH_2CH_2-$perylene), 1.73 (m, 4H, $-NCH_2CH_2-$), 1.87 (m, 4H, $-CH_2CH_2-$perylene), 4.15–4.22 (m, 8H, $-NCH_2(CH_2)_4CH_2-$perylene), 7.28–7.31 (m, 4H, aromatic protons), 7.51 (s, 4H, aromatic protons), 7.83–7.85 (d, J = 8.0 Hz, 4H, aromatic protons), 8.65 (s, 4H, aromatic protons). ^{13}C NMR ($CDCl_3$, ppm): 26.61, 26.79, 27.80, 28.57, 29.70, 43.42, 112.00, 114.23, 119.72, 121.31, 121.49, 122.58, 123.18, 123.28, 128.62, 132.99, 135.39, 141.34, 162.23. MASS (FAB): m/z 1344.

2.3. Synthesis of polymers

The synthesis of P3HT and hyperbranched polymers **P1**–**P4** is depicted in Scheme 3. All polymers were polymerized via the Universal Grignard metathesis polymerization [17]. The molar ratio of isopropylmagnesium chloride – lithium chloride (*i*-PrMgCl·LiCl) complex to monomer was controlled to 1.4:1. For polymers **P1**–**P4**, the molar ratio of two-headed monomers **M1**–**M4** to **M5** was controlled to 0.025:1. The detailed synthetic procedure of polymer **P1** was listed below as example.

To a mixture of **M1** (0.096 g, 0.076 mmol) and **M5** (1.0 g, 3.07 mmol) in 35 mL of anhydrous THF was added 1 M *i*-PrMgCl·LiCl (3.4 mL, 4.3 mmol) using syringe under nitrogen atmosphere. The reaction mixture was heated to 80 °C and stirred for 2 h. A dispersion of 1,2-bis(diphenylphosphinoethane)nickel(II)

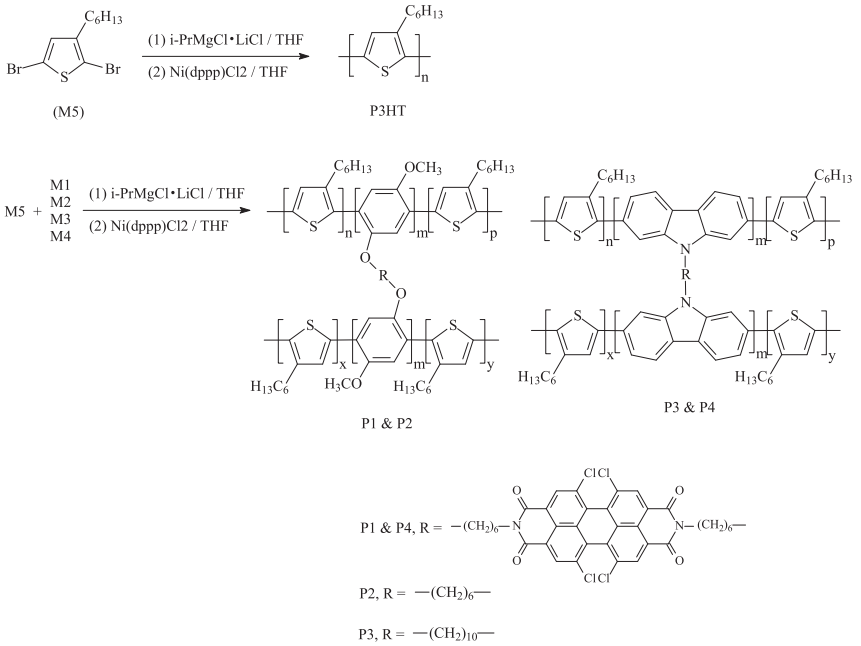

Scheme 3. Synthesis of P3HT and polymers **P1**–**P4**.

chloride (Ni(dppp)Cl_2) (9.0 mg, 1.66 × 10^{-2} mmol) in anhydrous THF (25 mL) was injected into the reaction mixture and stirred at 80 °C for 3 h. The resulting solution was then poured into 150 mL of MeOH and stirred for 1 h. The crude product was collected and re-precipitated in hexane several times to give a purple-black solid (0.206 g, 40%).

P3HT: by following the synthetic procedure of **P1** and using **M5** (1.0 g, 3.07 mmol), *i*-PrMgCl·LiCl (3.4 mL, 4.3 mmol), and Ni(dppp)Cl_2 (9.0 mg, 1.66 × 10^{-2} mmol) as starting materials, P3HT was obtained as a purple black solid (0.21 g, 41%).

P2: by following the synthetic procedure of **P1** and using **M2** (0.05 g, 0.076 mmol), **M5** (1.0 g, 3.07 mmol), *i*-PrMgCl·LiCl (3.4 mL, 4.3 mmol), and Ni(dppp)Cl_2 (9.0 mg, 1.66 × 10^{-2} mmol) as starting materials, **P2** was obtained as a purple-black solid (0.205 g, 40%).

P3: by following the synthetic procedure of **P1** and using **M3** (0.06 g, 0.076 mmol), **M5** (1.0 g, 3.68 mmol), *i*-PrMgCl·LiCl (3.4 mL, 4.3 mmol), and Ni(dppp)Cl_2 (9.0 mg, 1.66 × 10^{-2} mmol) as starting materials, **P3** was obtained as a purple-black solid (0.213 g, 41%).

P4: by following the synthetic procedure of **P1** and using **M4** (0.10 g, 0.076 mmol), **M5** (1.0 g, 3.68 mmol), *i*-PrMgCl·LiCl (3.4 mL, 4.3 mmol), and Ni(dppp)Cl_2 (9.0 mg, 1.66 × 10^{-2} mmol) as starting materials, **P4** was obtained as a purple-black solid (0.215 g, 41%).

2.4. Device fabrication and measurement

The P3HT and polymers **P1**–**P4** were firstly dissolved in dichlorobenzene (20 mg/mL). The solutions were then treated with ultrasonic treatment and heated at 70 °C for 30 min for better dissolution. The solutions were filtered and evacuated to extract the soluble part of the polymers. As for the fabrication of polymer solar cells, the polymer was blend with $PC_{60}BM$ in dichlorobenzene (1:2 in w/w) at a total concentration of 22.5 mg/mL, and the blend solution was stirred at 40 °C overnight. The blend solution was then spin-coated on a poly(3,4-ethylenedioxythiophene):poly(styrene sulfonate) (PEDOT:PSS, Clevios P VP AI4083)-coated ITO substrate to form a photoactive layer. The thickness of the photoactive layer was controlled to be 90–100 nm by adjusting the spin coating speed. The active layers were then treated with thermal annealing at 110 °C for 10 min, which is close to the glass transition temperature (T_g) of polymers. Finally, LiF (1.2 nm) and Al (70 nm) were deposited as cathode. Electrical characteristics were measured using a Keithley 2400 supplier. An AM 1.5 solar simulator (Oriel 96000 150 W) at 100 mW/cm^2 intensity was used for illumination measurements.

3. Results and discussion

3.1. Characterization of polymers

The goal of this research is to synthesize hyperbranched polythiophenes by incorporating two-headed monomers **M1**–**M4** during polymerization of P3HT. Both heads in **M1**–**M4** function as polymerizable monomers to extend polymer chains. Hyperbranched architectures of final polymers are expected to form with increased molecular weights and modified optoelectrical properties compared to the corresponding linear P3HT. The feed ratio of two-headed monomers should be low and well controlled to prevent gelation. In this study, the molar ratio of two-headed monomers to 2,5-dibromo-3-hexylthiophene (**M1**–**M4**:**M5**) is controlled to be 0.025:1 to ensure increased molecular weights and good solubility of final polymers in organic solvents, such as $CHCl_3$, chlorobenzene, or *o*-dichlorobenzene. The molecular weights of the synthesized polymers were determined by GPC, using linear polystyrenes as standards. It should be noted that the measured molecular weights of those hyperbranched polymers could be overestimated, since they are partially corsslinked and not linear polymers. Table 1 summarizes the number-average molecular

Table 1
Polymerization results of P3HT and polymers **P1**–**P4**.

Polymer	M_n (×10^{-4})	M_w (×10^{-4})	PDI
P3HT	1.69	3.16	1.87
P1	3.41	6.31	1.85
P2	2.92	5.42	1.86
P3	3.24	5.32	1.64
P4	2.82	5.62	1.99

weight (M_n), weight-average molecular weight (M_w), and polydipersity index (PDI) of synthesized polymers P3HT and **P1**–**P4** in this research. It is clearly seen that both M_n and M_w of hyperbranched polymers **P1**–**P4** are higher than those of P3HT, while PDI values are still less than 2. On the other hand, the structures of bridging moieties show insignificant effect on molecular weights of polymers (tetrachloroperylene bisimide v.s. alkyl spacer). As a result, the introduction of two-headed monomers brings increased molecular weights during polymerization of P3HT.

To examine the existence of bridging moieties in polymers, the ^{1}H NMR spectroscopy was performed and shown in Fig. 1. The proton signal on C-4 position of thiophene rings is observed at $\delta = 6.97$ ppm for P3HT, **P1**, and **P2**. In Fig. 1(a), a clear singlet at $\delta = 8.67$ ppm assigning to protons on perylene ring is found in **M1** and **P1**. Two specific signals at $\delta = 7.05$ and 3.81 ppm were assigned to protons on benzene ring and methoxy group for two-headed monomer **M1**, and those two signals are also found in corresponding hyperbranched polymer **P1**. Besides, the signals of $-OC\underline{H}_2$ and imide$-C\underline{H}_2$ from alkyl spacer between perylene and polymerizable head are also observed in **M1** and **P1**. Turning to Fig. 2(b), the proton signal from methoxy group at $\delta = 3.72$ ppm is clearly seen in **M2** and **P2**. Similar phenomena are found in polymers **P3** and **P4**, demonstrating that bridging moieties is successfully incorporated in polymers. The increased molecular weights of polymers are also supportive of this observation, as shown in Table 1.

3.2. Thermal properties of polymers

The TGA thermgrams of all polymers, including linear and hyperbranched ones, are shown in Fig. 2(a). All polymers show a first-stage weight loss above 300 °C, possibly due to the break of alkyl side chains or spacers. The main decomposition temperature (T_d) is observed above 450 °C, owing to thermal degradation of polymer main chains, which is consistent with the result of previous research [18]. It is noted that the weight loss of polymer **P1** is even smaller than that of P3HT and other polymers. The reason to this phenomenon can be explained by introduction of rigid perylene bisimide moieties and the highest molecular weights of **P1** among polymers. **P2** shows a similar TGA thermogram to that of P3HT. **P3** and **P4** owns lower T_d values and larger weight loss at same temperature.

The thermal transition behaviors, including T_g and melting point (T_m), are investigated by DSC in this study. The T_g of P3HT has been reported to be −14, 12, and 110 °C by different research groups [19–22], and T_m of P3HT was observed around 200–230 °C [22,23]. Since T_g is affected by molecular weights and structural regioregularity of polymers, the measurement of T_g of a certain P3HT can

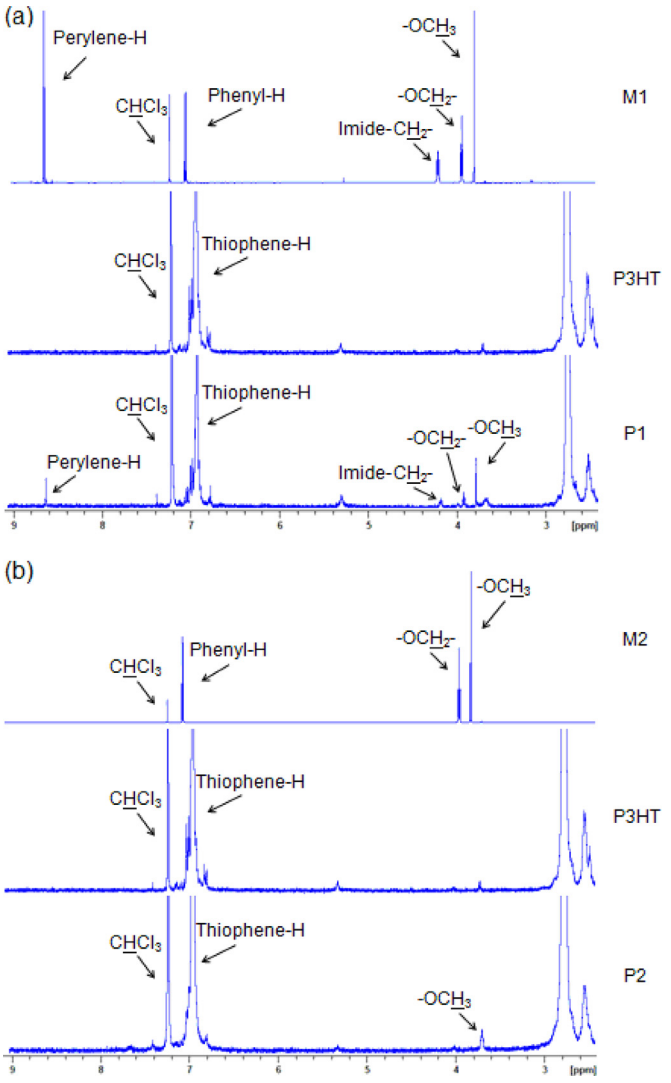

Fig. 1. ^{1}H NMR spectra of (a) **M1**, P3HT, and **P1**; (b) **M2**, P3HT, and **P2**.

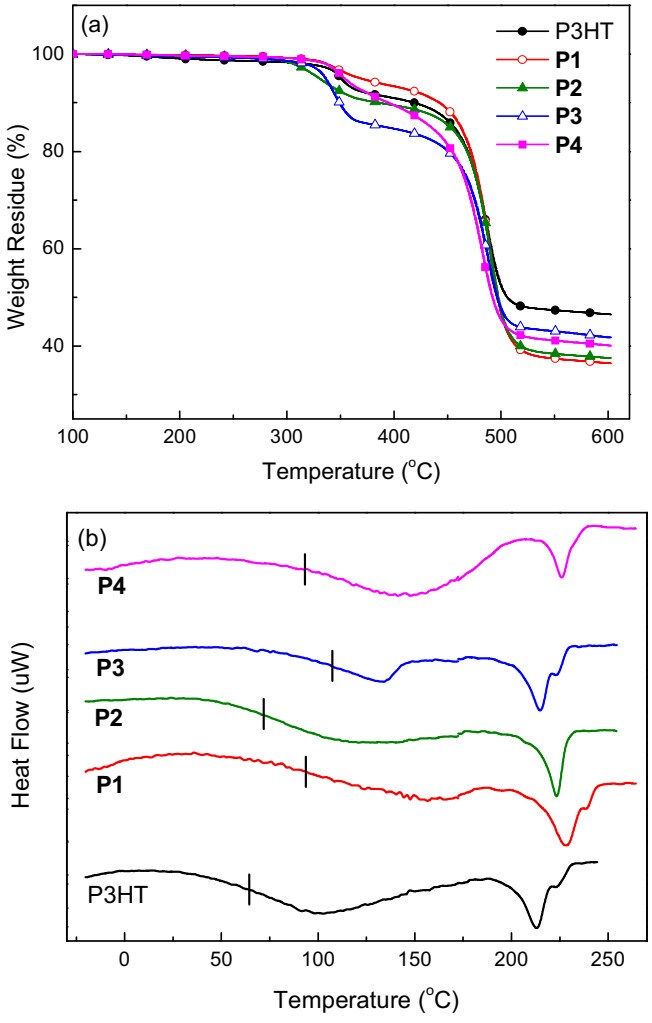

Fig. 2. (a) TGA and (b) DSC thermograms of P3HT and polymers **P1**–**P4**.

be varied with different material sources and characterization techniques. In this study, we strictly controlled polymerization condition of all polymers to evaluate the effect of two-headed monomers. The DSC thermgrams of P3HT and polymers **P1**–**P4** are shown in Fig. 2(b). The T_g and T_m of synthesized P3HT are observed at 67 and 213 °C, respectively. Furthermore, the T_g values of hyperbranched polymers **P1**–**P4** are found to be higher than that of P3HT (80–114 °C). This can be attributed to the hyperbranched architecture that prohibits segmental motions of polymer chains. The T_m values of polymers **P1**–**P4** are also higher than that of P3HT, as shown in Fig. 2(b). The above results reveal that better thermal stabilities of hyperbranched polythiophenes are achieved by introducing bridging moieties between polymer chains.

3.3. Optical properties of polymers

The UV–vis absorption spectra of all polymers are shown in Fig. 3. The solvent *o*-dichlorobenzene (*o*-DCB) is selected since it is often used for preparation of polymer solutions in solar cell applications. In Fig. 3(a), all polymers show a maximum absorption band centered at 465 nm in *o*-DCB, which is related to π–π* transition along polymer main chains. Besides, we notice a slight absorption shoulder around 520 nm for polymers **P1** and **P4** due to the presence of PBI moieties. In solid state, all polymers show a wide absorption band from 400 to 650 nm, with two characteristic absorption wavelengths located at 552 and 603 nm, as shown in Fig. 3(b). The former comes from π–π* transition along single polymer chain in solid state, and the latter is interpreted as aggregates of polymer chains. The spectral shapes and wavelengths of the synthesized polymers are both in accordance with those of regioregular P3HT reported in the literature [19,24]. Moreover, a stronger shoulder at 603 nm is found for those hyperbranched polymers compared to P3HT, implying reinforced interaction and closer aggregation between polymer chains brought by bridging moieties. The optical bandgap (E_g) of polymers can also be determined from the edge of UV–vis absorption in solid state in Fig. 3(b), giving E_g values of about 1.89–1.91 eV.

The normalized PL emission spectra of polymers were obtained by excitation at max absorption wavelength in different states, as shown in Fig. 4. The emission band centered at 589 nm for all polymers in *o*-DCB. An insignificant shoulder band can still be found around 640 nm, which is resulted from interchain interaction. On the other hand, polymers in thin film state show two emission maxima at 650 and 700 nm, referring to emissions from intra- and inter-chain behaviors, respectively [24]. Besides, the attenuated intensity of PL emission from P3HT to hyperbranced polymers, especially **P1**, is observed based on the same film preparation. The decreased emission in film state implies less possibility of carrier recombination and more opportunity for carriers to

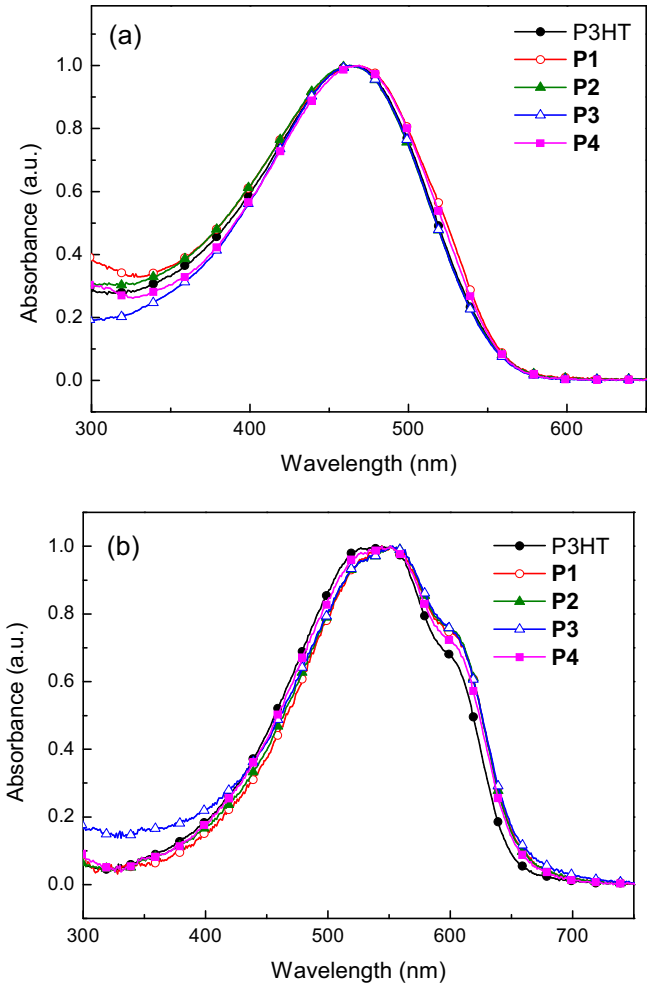

Fig. 3. UV–vis absorption spectra of P3HT and polymers **P1**–**P4** in (a) *o*-DCB and (b) thin film state.

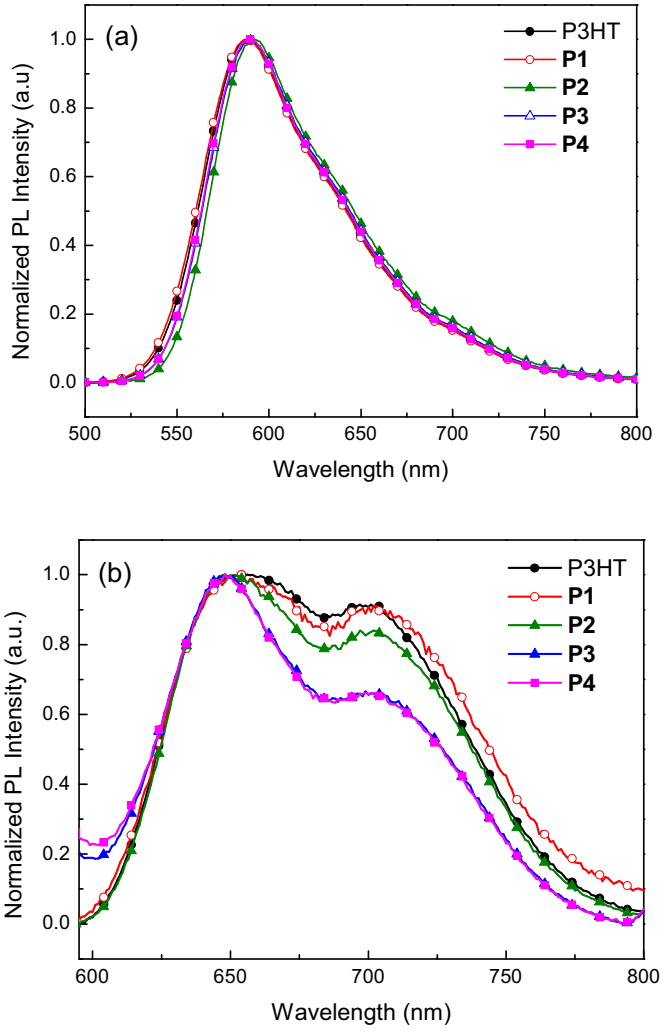

Fig. 4. Photoluminescent spectra P3HT and polymers **P1**–**P4** in (a) *o*-DCB and (b) thin film state.

migrate to both electrodes, which is a benefit for solar cell application.

3.4. Electrochemical properties of polymers

The CV voltammograms of all polymers in the oxidation scan are shown in Fig. 5(a). The onsets of oxidation potential (E_{ox}) of P3HT is found at 0.71 V, while **P1**–**P4** show higher oxidation onsets around 0.80–091 V. Besides, the energy bandgap (E_g) of polymer can be estimated from its absorption edge (λ_{edge}) in thin film state. The HOMO, E_g, and LUMO values are calculated from the following equations:

$$\mathrm{HOMO} = -|E_{ox} + 4.4|$$
$$E_g = 1240/\lambda_{edge}$$
$$\mathrm{LUMO} = -|\mathrm{HOMO} + E_g|$$

After calculation, the HOMO and E_g values of our synthesized P3HT are −5.11 and 1.91 eV, respectively, which are close to previous results in the literature [25]. For those hyperbranched polymers, the HOMO levels of **P1**–**P4** are in the range between −5.20 and −5.31 eV. The E_g values of **P1**–**P4** are 1.89 eV that are somewhat smaller than P3HT, since they possess longer absorption edges, as shown in Fig. 3(b). Combining HOMO levels and E_g values, the LUMO levels of polymers can be determined; the energy level diagram is then constructed and depicted in Fig. 5(b). The E_{ox}, HOMO, LUMO, and E_g values of all polymers are summarized in Table 2.

3.5. Device fabrication and evaluation of polymers

Solar cell devices with bulk heterojunction architecture were fabricated in the configuration ITO/PEDOT/donor:$PC_{60}BM$/LiF/Al.

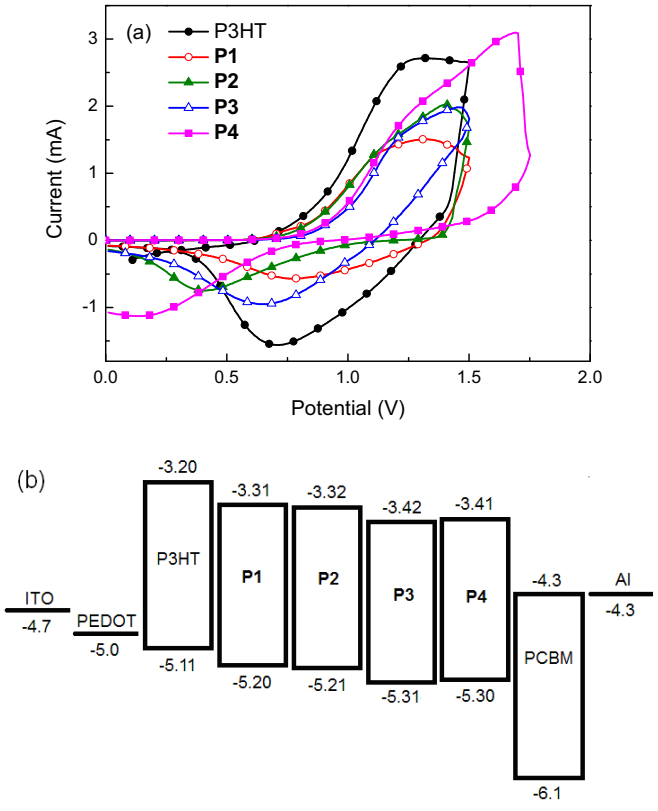

Fig. 5. (a) Cyclic voltammograms in the oxidation scan and (b) energy level diagram of P3HT and polymers **P1**–**P4**.

Table 2
Electrochemical properties of P3HT and polymers **P1**–**P4**.

Polymer	E_{ox} (V)[a]	HOMO (eV)[b]	LUMO (eV)[c]	E_g (eV)[d]
P3HT	0.71	−5.11	−3.20	1.91
P1	0.80	−5.20	−3.31	1.89
P2	0.81	−5.21	−3.32	1.89
P3	0.91	−5.31	−3.42	1.89
P4	0.90	−5.30	−3.41	1.89

[a] Data from CV in the oxidation scan.
[b] HOMO = − | E_{ox} + 4.4 |.
[c] LUMO = − | HOMO + E_g |.
[d] Data from the edge of the absorption spectrum in film state.

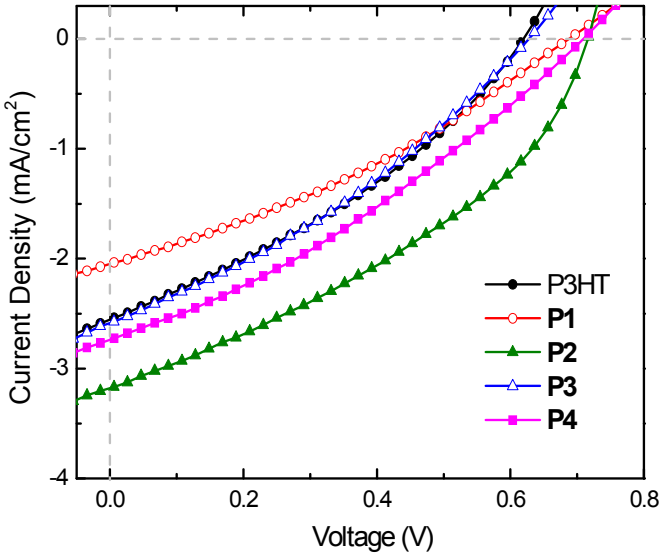

Fig. 6. Current density–voltage curves of the polymer solar cells based on P3HT and polymers **P1**–**P4** under AM 1.5 illumination, 100 mW/cm^2.

Hyperbranched PT derivatives and P3HT without bridging moiety were utilized as electron donor, and $PC_{60}BM$ was utilized as electron acceptor. The energy level diagram is shown in Fig. 5(b). The current density–voltage curves of these devices are shown in Fig. 6, and the summary of device performance is shown in Table 3. The devices utilizing hyperbranched PT derivatives as electron donor show larger V_{OC} than the one of P3HT reference cell. The V_{OC} is related to the difference between HOMO energy level of donor and LUMO energy level of acceptor [26]. The V_{OC} of P3HT device is 0.62 V which is consistent with previous reports [27]. It was reported that solar devices based on hyperbranched PTs showed higher V_{OC} values compared with normal P3HT [11]. In this study similar results are also found for polymers **P1**, **P2**, and **P4** which possess high V_{OC} values of 0.70–0.72°V. Larger V_{OC} of devices utilizing hyperbranched polythiophene derivatives can be attributed to the lower HOMO energy levels of hyperbranched polythiophene derivatives than the one of P3HT, resulting in larger difference

Table 3
Summary of cell characteristics based on P3HT and polymers **P1**–**P4** under one-sun illumination intensity.

Polymer	J_{SC} (mA/cm^2)	V_{OC} (V)	FF (%)	PCE (%)
P3HT	2.54	0.62	33.80	0.54
P1	2.03	0.70	32.04	0.45
P2	3.17	0.72	37.12	0.84
P3	2.57	0.64	32.02	0.52
P4	2.72	0.72	31.44	0.61

between HOMO energy level of the hyperbranched polythiophene derivatives and the LUMO energy level of $PC_{60}BM$.

Among devices utilizing hyperbranched polythiophene derivatives, both **P2** and **P4** devices perform better than P3HT device. **P2** device shows best performance and **P4** device is second best. The best performance of **P2** device is attributed to the larger V_{OC}, fill factor (FF), and J_{SC} values. Since the absorption spectra of all donor polymers are similar, such superior characteristics of **P2** device are believed to be related to its high carrier mobility and better molecular packing. Although the hole mobility of **P4** is larger than the one of **P2**, the rigid PBI moiety might hinder the packing of **P4** and the phase separation between **P4** and $PC_{60}BM$. Largest FF in **P2** device indicates a proper phase separation and a lowest carrier recombination among various devices. The hole mobilities of the synthesized P3HT and **P1**–**P4** in this study were determined by space-charge-limited current (SCLC) method (see Supplementary data). Hole-only devices with configuration of ITO/PEDOT:PSS/polymer/Au were fabricated and measured. The polymer **P2** possesses the highest hole mobility of 3.79×10^{-5} cm^2/V among all polymers, which is beneficial for carrier transport; meanwhile, other polymers own lower hole mobilities in the range of $1.02–1.88 \times 10^{-5}$ cm^2/V Fig. 7 shows AFM topographic images of polymer nanocomposite films blended with $PC_{60}BM$. The preparation of films for AFM analysis was identical to those used in device fabrication. It is seen that **P2**:$PC_{60}BM$ film shows the best distribution of aggregations among those films, revealing better charge dissociation between electron donors and acceptors. The root-mean-square roughness (Ra) of P3HT and **P1**–**P4** in blend with $PC_{60}BM$ was measured to be 16.7, 11.9, 8.29, 35.1, and 9.48 nm, respectively. The smallest roughness of **P2**:$PC_{60}BM$ blend

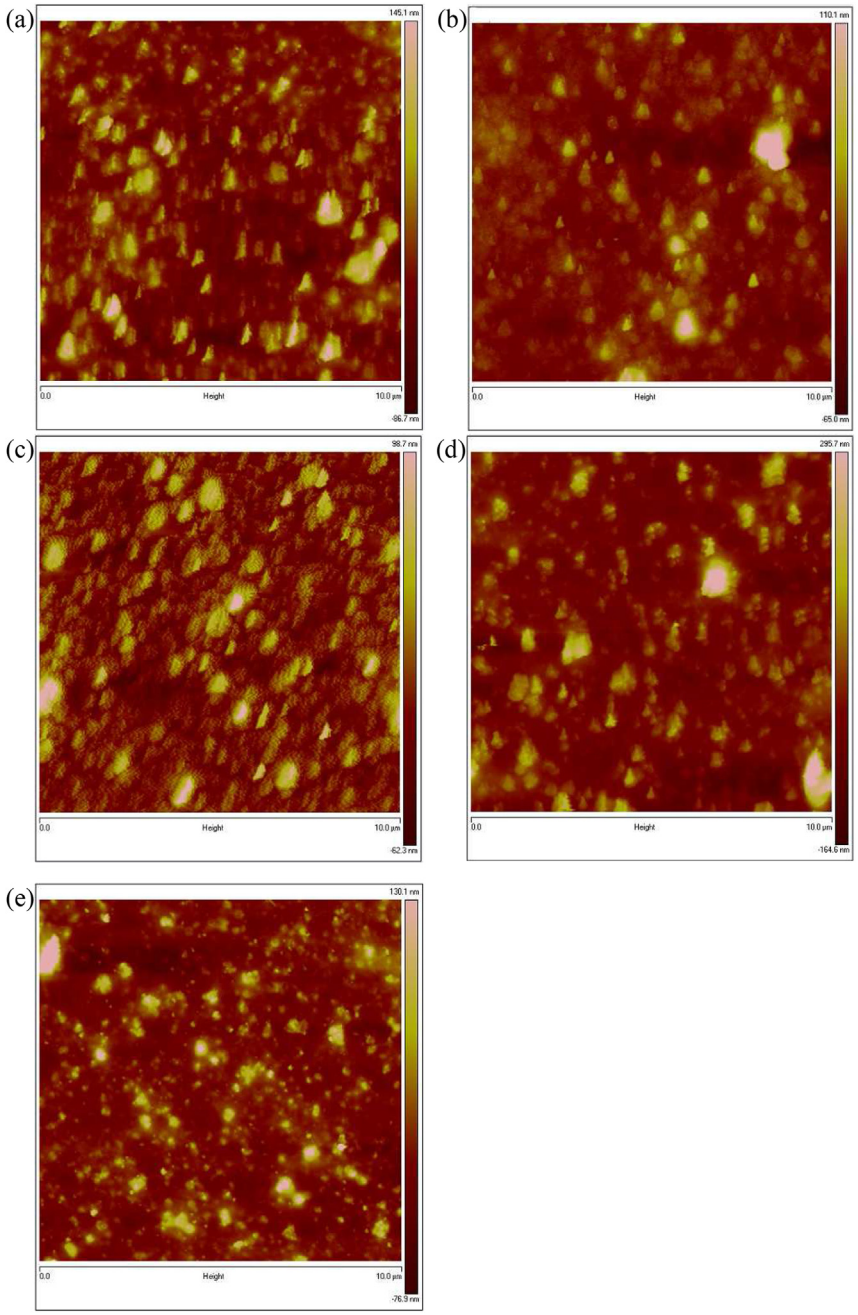

Fig. 7. AFM topographic images of (a) P3HT, (b) **P1**, (c) **P2**, (d) **P3**, and (e) **P4** in blend with $PC_{60}BM$.

represents good film quality that is also responsible for better device performance among those devices.

4. Conclusions

Hyperbranched PT derivatives containing tetrachloroperylene bisimide or alkyl spacer as bridging moiety were synthesized and characterized. The molecular weights and thermal stabilities of final polymers were increased by introducing hyperbranched architecture compared with normal P3HT. The intensity of shoulder band around 600 nm was increased for hyperbranched polymers, while their PL emissions were attenuated in thin film state. Solar devices based on those hyperbranched polymers blended with $PC_{60}BM$ showed PCE values of 0.45–0.84% and higher V_{OC} values up to 0.70–0.72 V than P3HT:$PC_{60}BM$ as active materials.

Acknowledgments

The authors thank the Ministry of Science and Technology (MoST) of the Republic of China (NSC 100-2113-M-009-012-MY2) for financial support of this research.

Appendix A. Supplementary data

Supplementary data related to this article can be found at http://dx.doi.org/10.1016/j.polymer.2014.09.046.

References

[1] Loewe RS, Khersonsky SM, McCullough RD. Adv Mater 1999;11:250–3.
[2] Loewe RS, Ewbank PC, Liu J, Zhai L, McCullough RD. Macromolecules 2001;34:4324–33.
[3] Lanzi M, Di-Nicola FP, Livi M, Paganin L, Cappelli F, Pierini F. J Mater Sci 2013;48:3877–93.
[4] Kim Y, Cook S, Tuladhar SM, Choulis SA, Nelson J, Durrant JR, et al. Nat Mater 2006;5:197–203.
[5] Vandewal K, Himmelberger S, Salleo A. Macromolecules 2013;46:6379–87.
[6] Cheng YJ, Yang SH, Hsu CS. Chem Rev 2009;109:5868–923.
[7] Chang YT, Hsu SL, Chen GY, Su MH, Singh TA, Diau EWG, et al. Adv Funct Mater 2008;18:2356–65.
[8] Chang YT, Hsu SL, Su MH, Wei KH. Adv Mater 2009;21:2093–7.
[9] Hou J, Tan Z, Yan Y, He Y, Yang C, Li Y. J Am Chem Soc 2006;128:4911–6.
[10] Lanzi M, Paganin L, Errani F. Polymer 2012;53:2134–45.
[11] Zhang Q, Cirpan A, Russell TP, Emrick T. Macromolecules 2009;42:1079–82.
[12] Zhou E, Tan Z, Yang Y, Huo L, Zou Y, Yang C, et al. Macromolecules 2007;40:1831–7.
[13] Tu G, Bilge A, Adamczyk S, Forster M, Heiderhoff R, Balk LJ, et al. Macromol Rapid Commun 2007;28:1781–5.
[14] Mangold HS, Richter TV, Link S, Würfel U, Ludwigs S. J Phys Chem B 2012;116:154–9.
[15] Schmidt R, Oh JH, Sun YS, Deppisch M, Krause AM, Radacki K, et al. J Am Chem Soc 2009;131:6215–28.
[16] Roncali J. Chem Rev 1997;97:173–205.
[17] Stefan MC, Javier AE, Osaka I, McCullough RD. Macromolecules 2009;42:30–2.
[18] Lee JU, Jung JW, Emrick T, Russell TP, Jo WH. J Mater Chem 2010;20:3287–94.
[19] Stevens DM, Qin Y, Hillmyer MA, Frisbie CD. J Phys Chem C 2009;113:11408–15.
[20] Zhao Y, Yuan G, Roche P. Polymer 1995;36:2211–4.
[21] Zhao J, Swinnen A, Assche GV, Manca J, Vanderzande D, Mele BV. J Phys Chem B 2009;113:1587–91.
[22] Kim Y, Choulis SA, Nelson J, Bradley DDC. Appl Phys Lett 2005;86:063502.
[23] Liao HC, Chantarat N, Chen SY, Peng CH. J Electrochem Soc 2011;158:E67–72.
[24] Brown PJ, Thomas DS, Köhler A, Wilson JS, Kim JS, Ramsdale CM, et al. Phys Rev B 2003;67:064203.
[25] Kim JY, Lee K, Coates NE, Moses D, Nguyen TQ, Dante M, et al. Science 2007;317:222–5.
[26] Nicholson PG, Castro FA. Nanotechnology 2010;21:492001.
[27] Zhao G, He Y, Li Y. Adv Mater 2010;22:4355–8.